International Journal of Microwave and Wireless Technologies

cambridge.org/mrf

Quantum-inspired sidelobe canceller beamformer with bidirectional beam scanning and sectorized jamming mitigation properties

Avishek Chakraborty[1], Indrasen Singh[2] and Chakradhar Adupa[3]

[1]School of Computer Science and Engineering, RV University, Bengaluru, India; [2]School of Electronics Engineering, Vellore Institute of Technology, Vellore, India and [3]Department of Electronics and Communication Engineering, SR University, Warangal, India

Research Paper

Cite this article: Chakraborty A, Singh I, Adupa C (2026) Quantum-inspired sidelobe canceller beamformer with bidirectional beam scanning and sectorized jamming mitigation properties. *International Journal of Microwave and Wireless Technologies* **18**(2), 183–198. https://doi.org/10.1017/S1759078726103195

Received: 11 June 2025
Revised: 8 April 2026
Accepted: 13 April 2026

Keywords:
beamformer; beamscanning; jamming; quantum algorithm; sidelobe canceller; time modulation

Corresponding author: Avishek Chakraborty; Email: avishekdreamz@gmail.com

Abstract

The proposed research aims to develop an efficient sidelobe canceller beamforming antenna array for scanning and anti-jamming purposes in radars with time-modulation. Time-modulated antennas are unconventional alternatives to phased arrays, in which the phase deviations between the impinging signals can be controlled by suitably switching ON and OFF the array elements at different time instants. This research addresses the design of a quantum-inspired optimal time-modulated beamformer, aiming for a broad scan coverage of 90° towards broadside. The scanned beams are generated using quantum algorithm-inspired time schemes, in which the ON times of each element are optimized to achieve the optimal radiation characteristics. The beamformer simultaneously aimed to suppress the sidelobes of the scanned radiation patterns. The proposed beamformer is designed for an 8-element antenna array, and the incorporation of time-modulation and its inherent harmonics generation enables simultaneous beam scanning over a desired region. The scanned patterns with reduced sidelobes are further exploited for the strategic null placement by proposing the time-modulated single-point anti-jammers. The concept is further extended, and an 8-element beamformer is developed for sectorized anti-jamming to show the efficiency, effectiveness, and robustness of the proposed research. Multiple sectors in the angular region are targeted by exploiting the harmonics and suppressing them below a desired level. The sidelobe canceller beamformer also demonstrates decent performance, suppressing sidelobes below 20 dB across all applications. The radiation power efficiency of the beamformer is more than 78%. The proposed sidelobe canceller time-modulated beamformer is also compared with other related research for a detailed comparison.

Introduction

The recent upswing in antenna research has heightened the need for efficient alternate methods of developing phased array antennas for advanced, cutting-edge applications, such as beamforming and beam steering. Due to the incorporation of "Time" as a fourth control parameter alongside the existing controls of amplitude, phase, and element spacing, time-modulated arrays have been proposed as potential substitutes for traditional antenna arrays [1]. The idea behind time-modulation is to regulate the ON and OFF switch timings of the array elements to produce the required phase divergence for phase tapering [2]. Shifted switching instants in a time-modulated antenna array can effectively support advanced adaptive beamforming applications with scanned patterns in predetermined directions [3]. Compared to traditional mechanical steering techniques, this electronic control can more effectively synthesize the radiating properties of the antenna [4]. In addition, these alternative arrays have the intrinsic advantage of having lower sidelobes with appropriate switching [5]. Due to the incorporation of the timing function, multiple sidebands or harmonic frequencies are produced by the Fourier transformation of coefficients from the time domain to the frequency domain [6]. Though the harmonics cause power loss in unwanted directions, they can also be exploited to generate multiple patterns simultaneously [7]. The possible exploitation of harmonics has been reported for electronic scanning, and new methods to create simultaneous beams have emerged [8, 9]. Initial research on time-modulation has shown substantial improvements in pattern synthesis by reducing sidelobes [10–12]. For efficiency enhancement, reducing sidelobes has become essential [13–15]. Controlling sidebands or harmonics and suppressing power in random directions also became a major research focus in time-modulation with the advent of optimization algorithms [16–20].

© The Author(s), 2026. Published by Cambridge University Press in association with The European Microwave Association.

In this context, shifting and splitting of time durations helped to lower the side beam power [21, 22]. The combination of shifted pulse and optimization algorithm has also been reported to simultaneously reduce sidelobes and sidebands [22–24]. In this respect, optimization methods helped achieve optimal time schemes to lower the higher-sideband power and the sidelobes of the main beam [25–27]. Optimization algorithms have also been employed to optimize the ON-time instants and the durations of the shifted and splitting pulses of time-modulated antennas for harmonic beam suppression [28–30]. In the later stages, other means of utilizing sideband radiation to create the desired multi-harmonic beam patterns have also emerged [31]. The advantages of simultaneously produced beams for multi-point transmission have also gained momentum [32–35]. Significant improvements in harmonic steering have been demonstrated through mathematical exploitation of the array phase center [36–38]. Time-modulated arrays are suitable for radar applications because of their electronic steering capability [39]. Monopulse radar application with concurrent sum-difference beams also became easier because a single optimized beamforming network can generate both beams using the inherent sidebands in time-modulation [40–42]. In addition, the concept has been used to develop several scanned beam patterns for multifunction radars with good scanning coverage [43]. Researchers have also focused on null placement across a wide angular region to further explore harmonic controlling for radars [44, 45]. Time-modulation has also been used for more advanced applications, such as shaped beam pattern generation [46–48], and for cognitive radios by exploiting its harmonics [49, 50]. Due to the adaptability and capabilities of optimized timing frameworks, time-modulated arrays have emerged as an efficient alternative to conventional phased arrays.

The research in this article further extended the time-modulation concept by proposing several optimal timing frameworks to generate an efficient sidelobe canceller beamformer for radars. The first objective is to design an adaptive sidelobe canceller beamformer that enables simultaneous multi-pattern scanning across different angular regions and suppresses the sidelobes of the scanned beams to a satisfactory level for interference rejection. The pulse-shifting and splitting methods, with optimized switch instants, are combined to generate optimal scanned beams for radar. The second objective is to place a deep null in a particular angular region to cancel out the transmission in that region by producing a zero-signal space for jamming. The third objective is the extended version of the second, in which sectorized anti-jamming is targeted using a single beamformer by controlling the harmonics. The objectives have been framed with real-time radar application in mind, where electronic beam scanning, sidelobe reduction, null control, and jamming mitigation are required. The specific objectives of this research, and the methods proposed for that, are elaborated as follows.

First, a time-modulated sidelobe canceller beamforming antenna is designed to suppress the interfering signals impinging on the sidelobes of the simultaneously scanned beams. The objective is to generate multiple scanned beams at prespecified directions ranging from 45° to 135°, covering a broad scanning area of around 90° in the broadside. For this purpose, the timing frameworks of an 8-element antenna are optimized so that the different optimized start instants of each antenna create a cumulative phase divergence in the overall radiation pattern. The mathematical foundation behind this approach is derived. The proposed beamformer can reduce sidelobes, and in the proposed research, the sidelobe levels (SLLs) of all scanned patterns are suppressed below 20 dB. Mathematically, the main beam consumes the maximum power in time-modulation. The first-harmonic beams on the positive and negative sides consume the second-largest power among the other higher harmonics. The scanning coverage is controlled by directing the first negative side beam toward 75°, 60°, and 45°, and the first positive side beam toward 105°, 120°, 135°, with scanning coverages of 30°, 60°, and 90°, respectively. The proposed beamformer also ensures that the SLLs of the scanned positive and negative beams, along with the main beam pattern, are below the standard levels for interference mitigation and unnecessary power radiation in random directions. The beamforming timing frameworks are employed with 8-element linear and symmetric time-modulated antenna arrays to validate the proposed approach.

Second, the adaptabilities of the beamformer are further tested for the strategic null placements in the direction of jammers. The strategic nulls can be placed by generating a zero-signal space in the broadside angular region so that the interfering signals can be efficiently blocked by concentrating only on the desired one. The proposed beamformer is aimed at placing nulls in a single direction as a single-point jammer, as well as for a sectorized jammer. The first-harmonic beam patterns are used to address the single nulls in the radiation pattern of an 8-element time-modulated antenna, while keeping the central beam constant. Two different cases are targeted by aiming the first-positive and first-negative harmonics toward null points at 40°, 60°, and 140°, 120°, respectively. To further extend the concept and to assess whether the proposed beamformer is adaptable enough to suppress signals across a broad region, sectorized jamming is targeted. Different cases of sectorized jamming are aimed at suppressing signals in the regions 0° to 65° and 40° to 80° using positive harmonics. Due to the symmetric nature of the linear array and the symmetry of the harmonics, the sectorized jamming is targeted from 115° to 180° and from 100° to 140°, with negative harmonics. The beamformer ensures the SLLs of all the patterns are below the standard requirements. The sectorized jamming targets signals below 30 dB across a broad region. For all scanning and jamming objectives, the central pattern is kept fixed in the broadside direction to optimize power usage. The efficient design of the beamformer also concentrates the maximum amount of power on the main beam and the first harmonic beams, thereby enhancing overall efficiency. For all the objectives, optimal switching instants and the ON time durations of the array ensure the efficiency of the proposed method. So, an efficient optimization method is needed to design an efficient time-modulated beamformer. The Particle Swarm Optimizer (PSO) has long been used to solve real-time engineering problems. PSO has also been rigorously applied to array radiation pattern synthesis. But it lacks efficiency and drastically increases the computation speed when too many objectives are targeted simultaneously. To overcome the limitations of PSO, a powerful quantum-inspired PSO is employed in this research to simultaneously optimize multiple objectives targeted by the proposed beamformer. The quantum-inspired PSO algorithm provides the much-needed efficient solutions for the beamformer and makes it a standout performer for efficient time-modulated radar systems.

The remaining part of the research is organized as follows: Section 2 describes the mathematical foundation of the time-modulated beamformer, where a detailed insight into a generalized time-modulated array and the incorporation of time schemes into its radiation pattern are provided. The construction of the symmetric array beamformer with pulse shifting and splitting, considering the effect of harmonics on radiation power efficiency, is also

https://doi.org/10.1017/S1759078726103195 Published online by Cambridge University Press

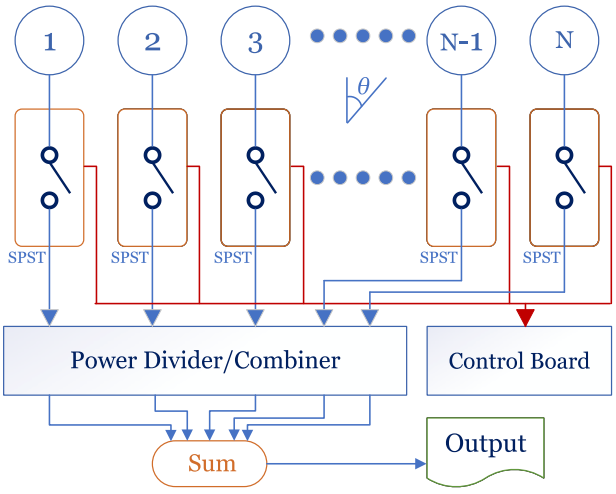


Figure 1. Generalized time-modulated beamforming structure with "*N*" antennas and switches.

formulated. The quantum-inspired PSO metaheuristic is presented in Section 3. The performance of the proposed beamformer as sidelobe canceller, single-point anti-jammer, and sectorized anti-jammers is analyzed in Section 4. The conclusive remarks and the future scopes are presented in Section 5.

Time-modulated beamformer design

Time-modulation includes a new control parameter, "Time", into the synthesis of array radiation patterns by mathematically modifying the array factor. The time-to-frequency domain conversion of the switching function provides an edge over traditional radiation pattern synthesis. The general mathematical modeling of the array response for an N-element symmetric linear antenna array connected with radio frequency (RF) switches, shown in Fig. 1, can be given as [02]

$$AF_S(\theta,t) = e^{(j2\pi f_0)t}.2\sum_{n=1}^{N/2}\left[I_n U_n(t)\, e^{\left\{j\beta\left(\frac{2n-1}{2}\right)d\cos\theta\right\}}\right] \quad (1)$$

The above expression shows the symmetric arrangement of "*N*" elements where the switching sequences of the elements in the left half are the same as the right half of the array elements. The beamformer in Fig. 1 shows "*N*" radiators connected to a power combiner via RF single-pole-single-throw (SPST) switches. The control board can provide the necessary tapering by controlling the ON and OFF timings of each radiator, and the responses from each radiator are summed to produce the synthesized radiation pattern. In equation (1), $U_n(t)$ represents the time-modulated switching sequences for each element from $n = 1$ to N, I_n is the current amplitude, f_0 denotes the central beam frequency, β is the wave propagation constant, d is the spacing between each radiator, signals are impinging at an angle θ to the array main axis, t represents the time instants within the modulation period, and $AF_{\text{Symmetric}}(\theta,t)$ stands for the overall array response after incorporating the time-modulation in a linear symmetric antenna array. Due to the periodicity of the timing function, $U_n(t)$ can be presented as [02]

$$U_n(t) = \sum_{m=-\infty}^{\infty}\left[a_{mn}e^{jm(2\pi f_p)t}\right] \quad (2)$$

Here, a_{mn} is the coefficient of excitation translated from the frequency to the time domain and represents the "*m*" number of frequency components for the *n*-th radiator. The frequency components, inherently generated by time-modulation, are called harmonics; where $m = 0$ represents the main beam, and $m = \pm1, \pm2, \pm3, \ldots, \pm\infty$ correspond to the sidebands at multiple positive and negative harmonics. The excitation coefficient a_{mn} at time-modulation frequency (f_p) with a modulation period T_p ($1/f_p$) can be extended as [02]

$$a_{mn} = \frac{1}{T_p}\int_0^{T_p} U_n(t)\, e^{-jm(2\pi f_p)t}\, dt \quad (3)$$

Putting the excitation coefficient into the antenna array response, the time-modulated response is modified as

$$AF_S(\theta,t) = e^{(j2\pi f_0)t}.2\sum_{n=1}^{N/2} I_n\left[\sum_{m=-\infty}^{\infty} a_{mn}e^{jm(2\pi f_p)t}.e^{\left\{j\beta\left(\frac{2n-1}{2}\right)d\cos\theta\right\}}\right] \quad (4)$$

Further, the simplified array response for the "*m*" number of frequency components can be presented as

$$AF_m(\theta,t) = e^{j2\pi(f_0\pm mf_p)t}.2\sum_{n=1}^{N/2}\left[I_n a_{mn}e^{\left\{j\beta\left(\frac{2n-1}{2}\right)d\cos\theta\right\}}\right] \quad (5)$$

The time-modulated array generates the central pattern at $m = 0$, and the harmonics are generated at $m = \pm1, \pm2, \pm3, \ldots, \pm\infty$. The main beam, the first positive and the first negative harmonics responses of the *N*-element array can be given as

$$AF_0(\theta,t) = e^{j2\pi(f_0)t}.2\sum_{n=1}^{N/2}\left[I_n a_{mn}e^{\left\{j\beta\left(\frac{2n-1}{2}\right)d\cos\theta\right\}}\right] \quad (6)$$

$$AF_{-1}(\theta,t) = e^{j2\pi(f_0-f_p)t}.2\sum_{n=1}^{N/2}\left[I_n a_{mn}e^{\left\{j\beta\left(\frac{2n-1}{2}\right)d\cos\theta\right\}}\right] \quad (7)$$

$$AF_{+1}(\theta,t) = e^{j2\pi(f_0+f_p)t}.2\sum_{n=1}^{N/2}\left[I_n a_{mn}e^{\left\{j\beta\left(\frac{2n-1}{2}\right)d\cos\theta\right\}}\right] \quad (8)$$

In this research, the first negative harmonics at $m = -1$ and the first positive harmonics at $m = +1$ are exploited for beam scanning and jamming in radars. Thus, it is very important to suppress higher harmonics and SLLs to conserve power and ensure efficient transmission and reception of the array. Furthermore, phase-divergence characteristics are also proposed for optimized shifted pulses in the beamformer, which need to be investigated for radiation pattern synthesis. Detailed mathematical modeling of power transmission and time-scheme modulation is also required to develop a multipurpose beamformer for scanning, jamming, and other advanced applications in modern radar systems.

Mathematical modeling of time schemes

The inherently generated side beams at multiple harmonics are generally considered a source of power loss but can be exploited for specific purposes. So, proper mathematical modeling is required to assess the sideband levels (SBLs) of the desired as well as higher-order harmonics. The closed-form derivatives of a simple pulse and a shifted pulse are derived in this subsection. The possible switching schemes are shown in Fig. 2(a) and (b), where Fig. 2(a)

https://doi.org/10.1017/S1759078726103195 Published online by Cambridge University Press

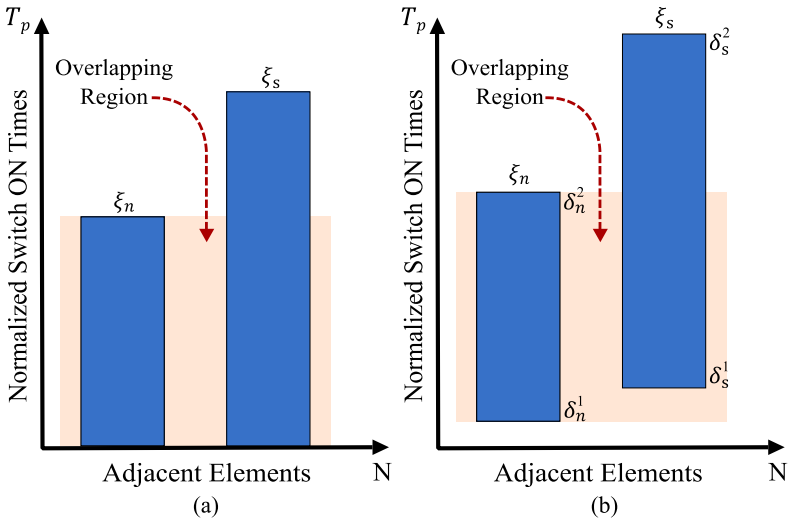


Figure 2. (a) Simplified time scheme and (b) Shifted pulse time scheme for the *n*-th and *s*-th adjacent elements.

shows a simple time scheme for two adjacent radiators, and Fig. 2(b) shows the same pulse scheme for shifted adjacent pulses. The first pulse scheme shows the *n*-th and *s*-th adjacent radiators with normalized time periods ξ_n and ξ_s within the modulating period (T_p), given by $\xi_n = (\tau_n/T_p)$ and $\xi_s = (\tau_s/T_p)$. The τ_n and τ_s are the time durations without normalization. The second scheme shows the shifted *n*-th and *s*-th pulses with normalized start instants δ_n^1 and δ_s^1. The pulses end at δ_n^2 and δ_s^2, respectively, within the modulation period. Figure 2 shows overlapping regions between adjacent time schemes, and the importance of these overlapping pulses is discussed in detail throughout the mathematical modeling of radiated power. Considering all the "*m*" harmonic responses, the overall array factor can be simplified from equation (4) as

$$AF_m(\theta,t) = \sum_{m=-\infty}^{\infty} |A_m(\theta)|\, e^{j2\pi(f_0 \pm mf_p)t} \tag{9}$$

$$\text{Here, } A_m(\theta) = 2\sum_{n=1}^{N/2} I_n a_{mn} e^{\left\{j\beta\left(\frac{2n-1}{2}\right)dcos\theta\right\}} \tag{10}$$

The total power transmission can be given as

$$\begin{aligned} P_T(\theta) &= \left\{\frac{1}{2}\sum_{m=-\infty}^{\infty} |A_m(\theta)|^2\right\} \\ &= \left\{\frac{1}{2}|A_0(\theta)|^2 + \frac{1}{2}\sum_{\substack{m=-\infty,\\ m\neq 0}}^{\infty} |A_m(\theta)|^2\right\} \\ &= P_0(\theta) + P_{SB}(\theta) \end{aligned} \tag{11}$$

Here, P_T, P_0, and P_{SB} are the total radiated power, main beam power, and harmonic beam power, respectively. The total power for "*m*" harmonics can further be expanded from equation (11) as

$$\begin{aligned} P_T = \int_0^{\pi} \frac{1}{2}\sum_{m=-\infty}^{\infty} |A_m(\theta)|^2 sin\theta\, d\theta &= \left\{\int_0^{\pi} \frac{1}{2}|A_0(\theta)|^2 sin\theta\, d\theta\right\} \\ &+ \left\{\int_0^{\pi} \frac{1}{2}\sum_{\substack{m=-\infty,\\ m\neq 0}}^{\infty} |A_m(\theta)|^2 sin\theta\, d\theta\right\} \end{aligned} \tag{12}$$

The first half of the above equation shows the power radiated by the main beam, and the second half describes the power in all the harmonic beams except the central pattern. Due to the complex characteristics of a_{mn} and the symmetries of harmonics, as they are always generated in pairs, such as positive and negative harmonics, $|A_m(\theta)|^2$ can be expanded as

$$\begin{aligned} |A_m(\theta)|^2 &= \{A_m(\theta)\}\{A_m(\theta)\}^* \\ &= \left[2\sum_{n=1}^{N/2} I_n a_{mn} e^{\left\{j\beta\left(\frac{2n-1}{2}\right)dcos\theta\right\}}\right] \\ &\times \left[2\sum_{n=1}^{N/2} I_n a_{mn} e^{\left\{j\beta\left(\frac{2n-1}{2}\right)dcos\theta\right\}}\right]^* \end{aligned} \tag{13}$$

For the *n*-th and *s*-th adjacent array elements without pulse shifting, the $|A_m(\theta)|^2$ can be generalized as:

$$\begin{aligned} |A_m(\theta)|^2 &= 4\sum_{n=1}^{N/2} |I_n a_{mn}|^2 \\ &+ 4\sum_{\substack{n,s=1\\ n\neq s}}^{N/2} \left[I_n I_s^* a_{mn} a_{ms}^* \left\{e^{j\beta\left(\frac{2n-1}{2}\right)(d_n - d_s)cos\theta}\right\}\right] \end{aligned} \tag{14}$$

The transformation of all the "m" harmonics is shown and also represented by a_{mn} and a_{ms} for the two adjacent radiators, where I_n, I_s are the current excitations and d_n, d_s are the spacing between the radiators, respectively. Putting the $|A_m(\theta)|^2$ expression into the total power (P_T) expression in equation (12)

https://doi.org/10.1017/S1759078726103195 Published online by Cambridge University Press

$$P_T = \int_0^{\pi} \frac{1}{2} \sum_{m=-\infty}^{\infty} \left[4 \sum_{n=1}^{N/2} |I_n a_{mn}|^2 + 4 \sum_{\substack{n,s=1 \\ n \neq s}}^{N/2} I_n I_s^* a_{mn} a_{ms}^* \left\{ e^{j\beta\left(\frac{2n-1}{2}\right)(d_n - d_s)cos\theta} \right\} \right] sin\theta \, d\theta \quad (15)$$

$$= \frac{1}{2} \sum_{m=-\infty}^{\infty} \left[4 \sum_{n=1}^{N/2} |I_n a_{mn}|^2 \int_0^{\pi} sin\theta \, d\theta + 4 \sum_{\substack{n,s=1 \\ n \neq s}}^{N/2} I_n I_s^* a_{mn} a_{ms}^* \int_0^{\pi} \left\{ e^{j\beta\left(\frac{2n-1}{2}\right)(d_n - d_s)cos\theta} \right\} sin\theta \, d\theta \right] \quad (16)$$

The above expression gives the total power in the main beam and all the symmetric positive and negative side beams. The side beam power ($m \neq 0$) can be extracted from the above expression as

$$P_{SB} = 2 \sum_{n=1}^{N/2} \left\{ |I_n|^2 \sum_{\substack{m=-\infty, \\ m \neq 0}}^{\infty} |a_{mn}|^2 \right\} + 4 \sum_{\substack{n,s=1 \\ n \neq s}}^{N/2} \left\{ Re\langle I_n I_s^* \rangle sinc\left[\beta\left(d_n - d_s\right)\right] \sum_{\substack{m=-\infty, \\ m \neq 0}}^{\infty} a_{mn} a_{ms}^* \right\} \quad (17)$$

To further simplify the power calculation for understanding the efficiencies of different pulse-scheme-based beamformers, a closed-form expression for the side beam power is required.

Harmonic power for shifted time scheme

The closed-form expression for the harmonic power may be simplified by considering the complex properties of a_{mn} and a_{ms} and summing up for the infinite number of harmonic frequencies as:

$$\sum_{\substack{m=-\infty, \\ m \neq 0}}^{\infty} a_{mn} \cdot a_{ms}^* = \sum_{\substack{m=-\infty, \\ m \neq 0}}^{\infty} a_{mn} \cdot a_{ms} \quad (18)$$

Considering uniform amplitudes ($I_n = 1$) and the shifted pulses shown in Fig. 2(b), a_{mn} can be derived as:

$$a_{mn} = \frac{1}{T_p} \int_{\tau_n^1}^{\tau_n^2} U_n(t) \, e^{-jm(2\pi f_p)t} \, dt = \frac{j}{2\pi m} \left[e^{-jm(2\pi\delta_n^2)} - e^{-jm(2\pi\delta_n^1)} \right] \quad (19)$$

The closed-form complex excitation for the adjacent radiators given in equation (18) can now be finalized by expanding the summation over the cosine series as:

$$\sum_{\substack{m=-\infty, \\ m \neq 0}}^{\infty} a_{mn} \cdot a_{ms}^* = \frac{1}{2} \left\{ \begin{array}{l} -|\delta_n^1 - \delta_s^1| + |\delta_n^1 - \delta_s^2| + |\delta_n^2 - \delta_s^1| - |\delta_n^2 - \delta_s^2| \\ -2\delta_n^1\delta_s^1 + 2\delta_n^1\delta_s^2 + 2\delta_n^2\delta_s^1 - 2\delta_n^2\delta_s^2 \end{array} \right\} = \frac{1}{2} \left\{ -|\delta_n^1 - \delta_s^1| + |\delta_n^1 - \delta_s^2| + |\delta_n^2 - \delta_s^1| - |\delta_n^2 - \delta_s^2| - 2\xi_n\xi_s \right\} \quad (20)$$

The above derivation in equation (19) can be simplified further by considering different possible combinations of start and finish instants for the n-th and s-th adjacent elements, based on the total ON-time duration of each. With two adjacent array elements and four switch ON and OFF instants, ${}^4C_2 = \frac{4!}{2!(4-2)!} = 6$ combinations of time schemes are possible. Combining all these possible conditions based on different ON and OFF times of the n-th and s-th elements, equation (20) can be simplified as:

$$\sum_{\substack{m=-\infty, \\ m \neq 0}}^{\infty} a_{mn} . a_{ms}^* = \left[\overline{\xi_{ns}} - \xi_n \xi_s \right] \quad (21)$$

Here, $\overline{\xi_{ns}}$ is the overlapping ON-time duration between two adjacent elements. The closed-form derivative of the sideband power for the shifted pulse switching scheme can finally be presented as:

$$P_{SB} = 2 \sum_{n=1}^{N/2} \{ [\xi_n (1 - \xi_n)] \} + 4 \sum_{\substack{n,s=1 \\ n \neq s}}^{N/2} \left\{ sinc\left[\beta\left(d_n - d_s\right)\right] \left[\overline{\xi_{ns}} - \xi_n \xi_s \right] \right\} \quad (22)$$

The closed-form approximation of the sideband harmonic power is useful for investigating the radiation power efficiency of the array. The radiation power efficiency can be measured as the ratio of radiated power in the desired directions to the total radiated power in all "m" harmonics, including the central beam and all the higher bidirectional symmetric harmonics. After deriving the radiation power efficiency and a closed-form derivative of the sideband harmonic beam power for the shifted pulse scheme, the next step is to design a time-modulated beamformer that generates the pulse-shifting instants for all elements to scan a specific region.

Derivation of shifting instants for scanning

To derive the starting instants of each element in a time-modulated array for the required phase shift effect, the complex excitation response of the antenna array can be modified from equation (19) as:

$$a_{mn} = \frac{j}{2\pi m} \left[e^{-jm(2\pi\delta_n^2)} - e^{-jm(2\pi\delta_n^1)} \right] = (\delta_n^2 - \delta_n^1) \frac{[sin\{m\pi(\delta_n^2 - \delta_n^1)\}]}{[m\pi(\delta_n^2 - \delta_n^1)]} e^{-jm\pi(2\delta_n^1 + \xi_n)} = (\delta_n^2 - \delta_n^1) [sinc\{m\pi(\delta_n^2 - \delta_n^1)\}] \, e^{-jm\pi(2\delta_n^1 + \xi_n)} \quad (23)$$

https://doi.org/10.1017/S1759078726103195 Published online by Cambridge University Press

The simplified expression for a_{mn} for the shifted pulse time scheme can affect the overall array response as:

$$AF_m(\theta,t) = e^{j2\pi(f_0\pm mf_p)t}.2\sum_{n=1}^{N/2}(\delta_n^2-\delta_n^1)\left[sinc\left\{m\pi(\delta_n^2-\delta_n^1)\right\}\right] \times e^{-jm\pi(2\delta_n^1+\xi_n)}e^{j\beta\left(\frac{2n-1}{2}\right)dcos\theta} \quad (24)$$

$$= e^{j2\pi(f_0\pm mf_p)t}2.\sum_{n=1}^{N/2}(\delta_n^2-\delta_n^1)\left[sinc\left\{m\pi(\delta_n^2-\delta_n^1)\right\}\right] \times e^{j\left[\left\{\beta\left(\frac{2n-1}{2}\right)dcos\theta\right\}-\left\{m\pi(2\delta_n^1+\xi_n)\right\}\right]} \quad (25)$$

The final array factor expressions for the central beam and first-order harmonic beams can be represented as

$$AF_0(\theta,t) = e^{j2\pi(f_0)t}.2\sum_{n=1}^{N/2}(\delta_n^2-\delta_n^1)e^{j\beta\left(\frac{2n-1}{2}\right)dcos\theta} \quad (26)$$

$$AF_{-1}(\theta,t) = e^{j2\pi(f_0-f_p)t}.2\sum_{n=1}^{N/2}(\delta_n^2-\delta_n^1)\left[sinc\left\{\pi(\delta_n^1-\delta_n^2)\right\}\right] \times e^{j\pi f_p(2\delta_n^1+\xi_n)}e^{j\beta\left(\frac{2n-1}{2}\right)dcos\theta} \quad (27)$$

$$AF_{+1}(\theta,t) = e^{j2\pi(f_0+f_p)t}.2\sum_{n=1}^{N/2}(\delta_n^2-\delta_n^1)\left[sinc\left\{\pi(\delta_n^2-\delta_n^1)\right\}\right] \times e^{-j\pi f_p(2\delta_n^1+\xi_n)}e^{j\beta\left(\frac{2n-1}{2}\right)dcos\theta} \quad (28)$$

It is clear from equation (25) that the time-modulated array with a shifted time scheme incorporates a specific term in the antenna response, i.e., $e^{j\left[\left\{\beta\left(\frac{2n-1}{2}\right)d\cos\theta\right\}-\left\{m\pi(2\delta_n^1+\xi_n)\right\}\right]}$, responsible for the static phase distribution with a delay. So, a phase divergence can be implemented by controlling the two parameters δ_n^1 and ξ_n $(=\delta_n^2-\delta_n^1)$ by maintaining the other parameters as constants. To elaborate further and to measure the starting instants (δ_n^1) of each element, the aforementioned phase-divergence expression can be set to zero, as $e^0 = 1$ yields uniform phase deviation for the impinging array signals. This shows an extra advantage of time-modulation, as no external phase shifters are needed to provide the necessary deviation required for the scanning or steering performance. The starting instant (δ_n^1) can be calculated by taking $e^{j\left[\left\{\beta\left(\frac{2n-1}{2}\right)d\cos\theta\right\}-\left\{m\pi(2\delta_n^1+\xi_n)\right\}\right]} = 1$, which shows that a uniform and static phase distribution is applied. The phase distribution can be simplified by deriving the δ_n^1 for a prespecified angle θ_0 as

$$\delta_n^1 = \left[\frac{\beta(2n-1)\,dcos\theta_0}{4m\pi} - \frac{\xi_n}{2}\right] \quad (29)$$

Using the above derivation, the pulse-shifting instants, or the shifted ON-times of each element, may be derived to scan the m-th harmonics at a prespecified direction θ_0. The research in this article specifically focuses on designing a time-modulated beamformer by exploiting the first harmonic beams as the first harmonics contain most of the power following the central beam pattern. So, the above derivation can be generalized for the first positive and the negative harmonics $(m = \pm 1)$ as

$$\delta_n^1 = \left[\frac{\beta(2n-1)\,dcos\theta_0}{4\pi} - \frac{\xi_n}{2}\right] \bmod 1 \quad (30)$$

Here, mod denotes the module operation, used to describe the symmetric nature of the harmonic beams $(m = \pm 1)$. After modeling the shifting times to scan the first-order harmonics toward θ_0, the next step of the design process is to optimize the ON-time durations ξ_n $(=\delta_n^2-\delta_n^1)$ or the time periods of each element of the array. Controlling ξ_n can reduce the SLLs of the radiation patterns; for this, a quantum-approximated optimization technique is adopted in this research. Further, the higher-order harmonic beams can also be suppressed if the beamformer is properly optimized.

Quantum-inspired optimization

The quantum-inspired metaheuristic algorithm is employed in this research to design an optimized beamformer that cancels interferences by suppressing SLLs. The SLCB proposed in this research is designed specifically for radar scanning and anti-jamming. So, suppressing SLLs across all scanned or steered patterns is absolutely necessary. Parameters like SLLs of the main beam and the first side beams, along with all the other higher SBLs, are aimed to be suppressed using optimization algorithm. The popular, well-known swarm-intelligence-based PSO algorithm has long been used to solve real-world engineering problems. It has also been rigorously applied to antenna beam pattern synthesis [51, 52]. However, it is inefficient when multiple objectives are targeted simultaneously. A more powerful quantum-based PSO is employed in this research to achieve multiple objectives of the beamformer.

PSO was originally proposed by Kennedy and Eberhart in 1995 [53]. This population-based swarm intelligence optimization algorithm was inspired from the properties of fish schooling or bird flocking. The particles of a population of size "N" usually move around in the multi-dimensional or "D" dimensional search space to find optimal and suboptimal solutions, based on some mathematical modeling that analyses the trajectories of each particle in terms of its velocity and position. In a traditional or classical PSO, the velocity (v_i) and position (x_i) of the i^{th} $(1 \leqslant i \leqslant N)$ particle at some iteration instant t can be presented Kennedy and Eberhart [53]

$$v_i(t) = \left[v_{i,1}(t),\, v_{i,2}(t),\, v_{i,3}(t),\, \ldots,\, v_{i,D}(t)\right] \quad (31)$$

$$x_i(t) = \left[x_{i,1}(t),\, x_{i,2}(t),\, x_{i,3}(t),\, \ldots,\, x_{i,D}(t)\right] \quad (32)$$

The trajectories of the i^{th} particle in terms of its velocity and position are updated as follows [53]:

$$v_{i,d}(t+1) = \left\{w.v_{i,d}(t)\right\} + \left\{c_1.rand_1.\left(pbest_{i,d}(t) - x_{i,d}(t)\right)\right\} + \left\{c_2.rand_2.\left(gbest_d(t) - x_{i,d}(t)\right)\right\} \quad (33)$$

$$x_{i,d}(t+1) = x_{i,d}(t) + v_{i,d}(t+1) \quad (34)$$

Here, w is the weight of inertia, $v_{i,d}(t+1)$ is the updated velocity of the i^{th} particle for the d^{th} $(1 \leqslant d \leqslant D)$ dimension, $x_{i,d}(t+1)$ is the updated position, c_1, c_2 are the learning coefficients, $rand_1$, $rand_2$ are random numbers $\in (0,1)$, $pbest_{i,d}(t)$ gives the best position of the i^{th} particle for d^{th} dimension at t^{th} iteration, and $gbest_d(t)$ denotes the best of all the "N" particles for d^{th} dimension. Now, each particle will converge to its best position if the upper limit $\varphi_{k,d}$ is properly selected. The best convergence of each particle can be denoted by Kennedy and Eberhart [54]

$$p_i(t) = \left[p_{i,1}(t), p_{i,2}(t), p_{i,3}(t), \ldots, p_{i,D}(t)\right] \quad (35)$$

Here, $p_{i,d}(t) = \frac{\{(\varphi_{1,d}*pbest_{i,d}(t))+(\varphi_{2,d}*gbest_d(t))\}}{(\varphi_{1,d}+\varphi_{2,d})}$ and $\varphi_{1,d}$, $\varphi_{2,d} \in (0,1)$ are uniformly distributed [55].

https://doi.org/10.1017/S1759078726103195 Published online by Cambridge University Press

In classical mechanics, the trajectory of a particle in the search space can be determined by its velocity vector $\vec{v}$ and position vector $\vec{x}$. The particle can move along this trajectory according to Newtonian mechanics, but in the quantum regime, it does not have a trajectory, as the simultaneous determination of $\vec{v}$ and $\vec{x}$ is not possible due to the *uncertainty principle* [54]. The particle in a quantum-inspired PSO moves within the potential field, exhibiting bound-state behavior. Among various potential field models in quantum mechanics, *Delta Potential Well* is one of the simplest and most elegant models, giving one bound state with a finite energy, a localized wave function, and confinement to a region. The quantum state of the particle moving in the *Hilbert space* can be represented by wave function $\psi(x,t)$. The *Delta Potential Well* has a sharp, localized effect, with only one bound state because of the specific nature of a delta function, which allows only one state to exist. More precisely, in a *Delta Function* $\delta(x)$, the value is zero everywhere except at $x = 0$, and the integral value over the range is unity, which may be shown as follows [54]:

$$\delta(x) = \begin{cases} \infty, & x = 0 \\ 0, & x \neq 0 \end{cases} \quad \text{and} \quad \int_{-\infty}^{\infty} \delta(x)\, dx = 1 \tag{36}$$

Considering the particle in one-dimensional space, the *delta potential* in its ideal form can be given as [54]

$$V(x) = -\alpha\delta(x) \tag{37}$$

Here, α is a positive coefficient that represents the strength of the potential field analogous to the depth of the *Delta Potential Well*, and $\delta(x)$ denotes the *Dirac Delta Function* that represents a potential with finite strength having an infinitely narrow response at $x = 0$. To achieve the bound state in a potential well, the energy of the particle must be less than zero ($E < 0$). In a bound state, the particle is confined or trapped within the potential well and is unable to escape the well unless energy is supplied. It shows that, in the bound state, due to the negative energy, the particle is trapped and the wave function $\psi(x,t)$ is localized around the potential. The *wave function* $\psi(x)$ at a particular instant decay exponentially away from $x = 0$, which reflects the fact that the particle has maximum probability of occurrence near the potential well and that the probability decreases far from the well. Now, assuming all the particles of PSO are under a *quantum potential well* and attracted towards a center point $p_{i,d}(t)$ for best convergence, the updated position of the i^{th} particle sampled from the probability distribution around $p_{i,d}(t)$ can be given Agarwal et al. [55]

$$x_{i,d}(t+1) = p_{i,d}(t) \pm \frac{L_{i,d}(t)}{2} ln\left(\frac{1}{u_{i,d}(t)}\right) \tag{38}$$

Here, $u_{i,d}(t)$ is the uniform random number $\in (0,1)$, and $L_{i,d}(t)$ represents the dynamically adjusted potential well length around the mean best position of the i^{th} particle in the *quantum potential well*, given by Agarwal et al. [55]

$$L_{i,d}(t) = 2\beta.\left|mbest_d(t) - x_{i,d}(t)\right| \tag{39}$$

Here, β is the *contraction-expansion parameter* that gradually decreases over time to ensure good exploration at the initial stage and better exploitation at later stages for optimal fine-tuning of the solution. Putting the above expression in equation (38), the final position update equation of quantum-inspired PSO becomes [55]:

$$x_{i,d}(t+1) = p_{i,d}(t) \pm \beta.\left|mbest_d(t) - x_{i,d}(t)\right|.ln\left(\frac{1}{u_{i,d}(t)}\right) \tag{40}$$

The final expression shows that, in quantum-inspired PSO, only the parameter β needs to be controlled, rather than w, c_1, and c_2 in classical PSO. The major advantage is that no velocity update expression is required to update the position of a particle, which further simplifies the optimization process by providing quicker results and avoiding the risk of trapping in local optimum. These added advantages ultimately help to achieve multiple objectives within a short time period.

This research on time-modulated arrays also deals with multiple objectives, such as SLL canceller for the main beam and the harmonics, steering the first harmonics efficiently so that other higher harmonics are suppressed, placing a single null in prespecified directions for anti-jamming, along with sectorized jamming mitigation by maintaining decent SLLs for all the desired beam patterns. In this regard, the timing instant and period of each antenna in the array play the most important roles, and the mathematical modeling presented in the earlier section also supports this. To optimize the performance using quantum-inspired PSO algorithm, all the desired objectives of the proposed research are framed into a single objective function as follows:

$$\Psi\langle\xi_n\rangle = \left[\prod_{i=1}^{N}\left\{w_{SLL}\left(H\left[\widetilde{SLL} - SLL\langle\xi_n\rangle\right]\frac{\left|\widetilde{SLL} - SLL\langle\xi_n\rangle\right|^2}{\left|\widetilde{SLL}\right|^2}\right)\right\}\right]_{\substack{m=0\\ m=\pm1}} + \left[\prod_{i=1}^{N}\left\{w_{SBL}\left(\frac{P_{SB}\langle\xi_n\rangle}{P_T\langle\xi_n\rangle}\right)\right\}\right]_{\substack{m\neq0\\ m\neq\pm1}} \tag{41}$$

The first part in the above equation tries to cancel out the sidelobes for the main beam ($m = 0$) and the first side beams ($m = \pm1$) by calculating over all the iterations ($i = 1, 2, 3, \ldots, N$), where $\widetilde{SLL}$ is the desired level of sidelobes and $SLL\langle\xi_n\rangle$ shows the actual level of sidelobes generated after a particular i^{th} iteration for $m = 0, \pm1$. $H(\cdot)$ is the Heaviside step function designed for sudden changes in SLLs. The second part completely deals with the suppression of higher side beams generated at an infinite number of harmonic frequencies except $m = 0, \pm1$, i.e., for all the harmonics from $m = \pm2$ to infinity. The aim is to address these multiple objectives within a single optimization framework using the quantum-inspired PSO.

Results and analysis

The research aims to design an efficient sidelobe-canceller beamforming network (BFN) that incorporates the time-modulation concept for electronic beam scanning and jamming in radars. The mathematical modeling of the time-modulated beamformer is derived in the earlier sections. The main controlling parameters of the array beamformer are the switching instants (δ_n^1) and the ON-time durations (ξ_n) of each element. The mathematical prospect of an 8-element beamformer with shifted time instants and optimized ON durations of each element is modeled with a quantum-inspired PSO algorithm. The performance of the proposed 8-element beamforming array in achieving multiple goals is discussed in the following subsections.

https://doi.org/10.1017/S1759078726103195 Published online by Cambridge University Press

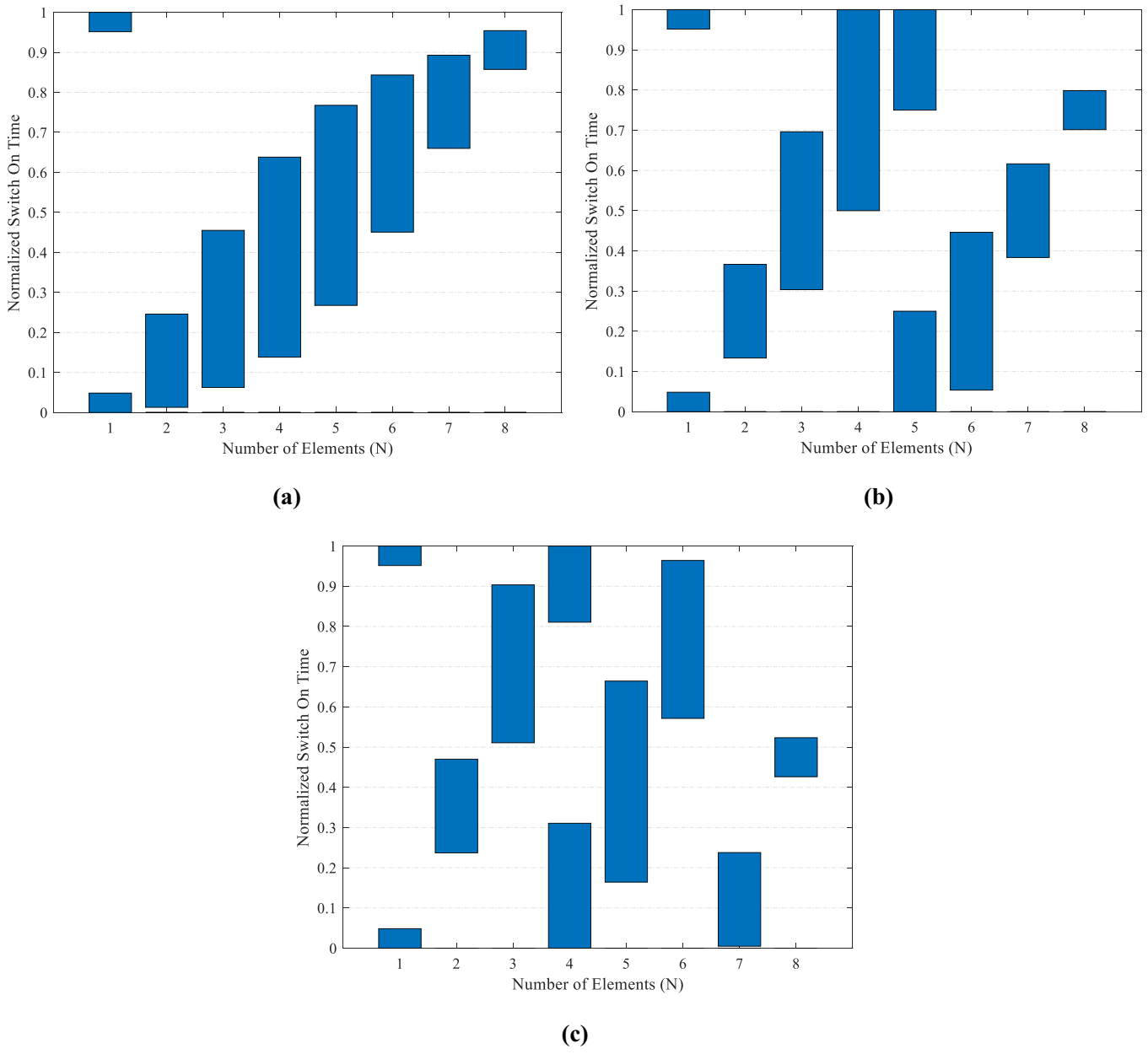


Figure 3. Optimized sidelobe cancelling beamforming time schemes for (a) ±15°, (b) ±30°, and (c) ±45° scanned beams.

Sidelobe canceller beam scanner

The quantum-inspired 8-element time-modulated beamformer array is intended to suppress interfering signals arriving at or transmitted from the sidelobes. It also creates simultaneous scanned beam patterns at prespecified directions between 45° and 135°, covering a broad angular region of 90° in the broadside. To design a sidelobe-canceller beamformer, the mathematically derived shifted time instant in equation (38) is used to obtain the normalized starting instant (δ_n^1) for each element, and the normalized ON-time duration (ξ_n) of the array is optimized using the single-objective function in equation (41). The desired level of projected $\widetilde{SLL}$s across all radiation patterns is set to −20 dB. The quantum-optimized starting instants (δ_n^1) and the time duration of each element constitute the optimal beamforming time scheme, which ultimately includes the desired cumulative phase deviation in the overall array radiation pattern. Three different scanning performance cases are aimed at exploiting the first-harmonic beams while keeping the main beam constant in the broadside direction. In Case 1, the scanned harmonic beam patterns are targeted toward 75° and 105°, i.e., 15° deviated from the broadside using the first negative and first positive harmonics ($m = \pm 1$). To check the adaptiveness of the proposed beam scanner, the first negative and first positive harmonics are also steered toward 60°, 45°, and 120°, 135° in Cases 2 and 3, respectively. The optimal time schemes for all different pairs of scanned beams are given in Fig. 3(a), (b), and (c). The sidelobe-canceller scanning patterns generated with the optimal switching schemes are shown in Fig. 4(a), (b), and (c). In Fig. 3(a), the beam scanner is designed to scan the first harmonics to 75° and 105°, and the corresponding radiation characteristics, presented in Fig. 4(a), shows that the goal is achieved

https://doi.org/10.1017/S1759078726103195 Published online by Cambridge University Press

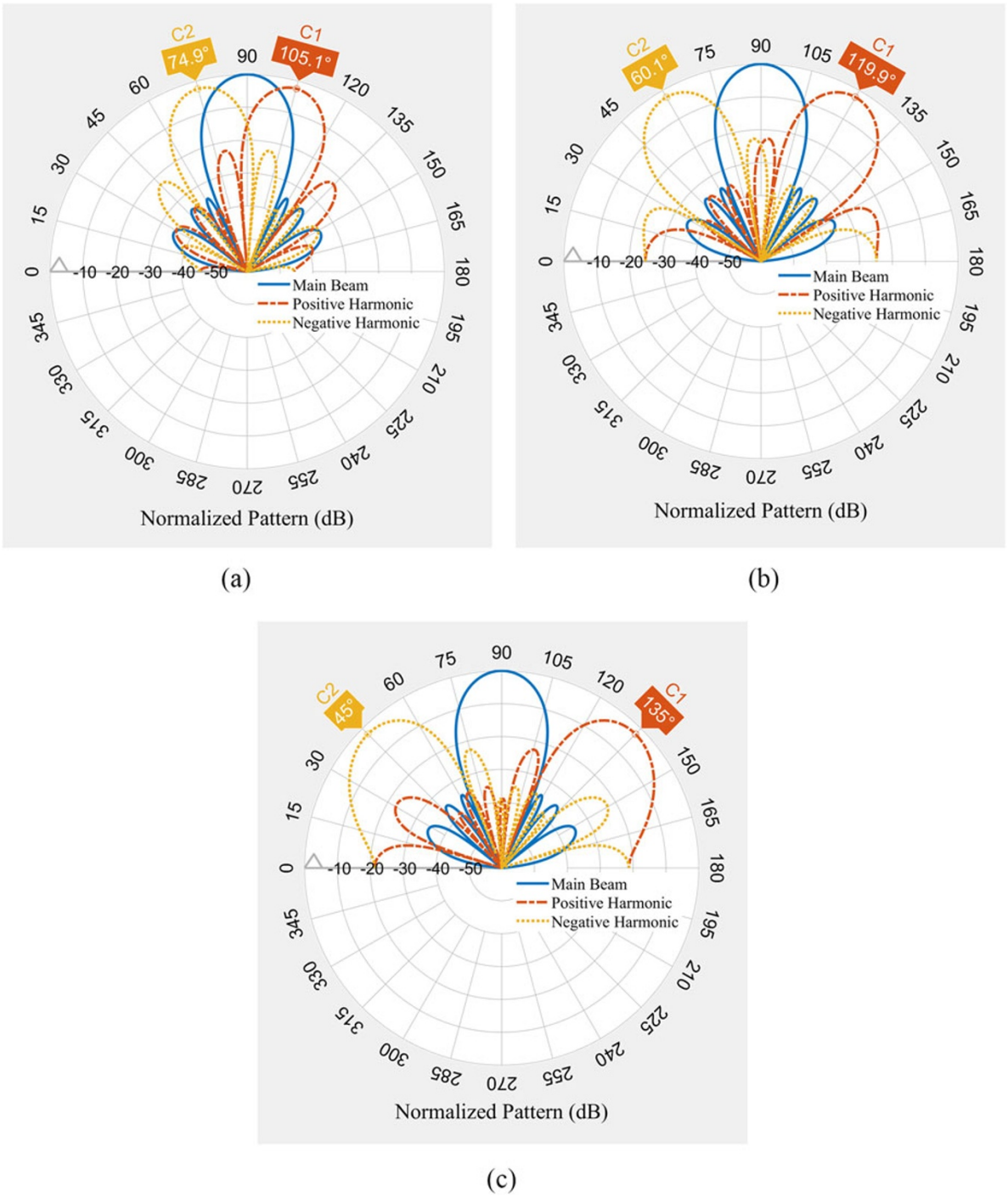


Figure 4. Optimized time-modulated beam scanning patterns with (a) ±15°, (b) ±30°, and (c) ±45° scanned beams.

by pointing the first negative harmonics at 74.89° and the first positive harmonics at 105.11°. Similarly, the desired goals of Case 2, with scanned beams toward 60° and 120°, are also achieved by the optimal time scheme presented in Fig. 3(b). The scanned beams are pointed at 60.11° and 119.89°, as shown in Fig. 4(b). In Case 3, the scanning patterns at 45° and 135° are also achieved with the quantum-inspired optimal time scheme given in Fig. 3(c), and the corresponding scanned patterns are validated in Fig. 4(c).

The SLLs for the main beams, created along with the scanned beams, are suppressed to −34.8 dB, which shows an impressive improvement over the −13 dB SLL of the uniform array pattern (without optimizing ξ_n). The SLLs of the first harmonics are also reduced to −22.8 dB, which provides convincing performance against the targeted objective of −20 dB $\widetilde{SLL}$ for interference rejection. Only the central pattern and the first harmonic patterns are exploited to achieve the desired beam-scanning objectives. To show that the optimized beamformer creates power-efficient beam-scanning radiating patterns, all higher-harmonic beams, except the first, are also reduced. The higher-order harmonics are suppressed as an effect of the second part of the constructed

https://doi.org/10.1017/S1759078726103195 Published online by Cambridge University Press

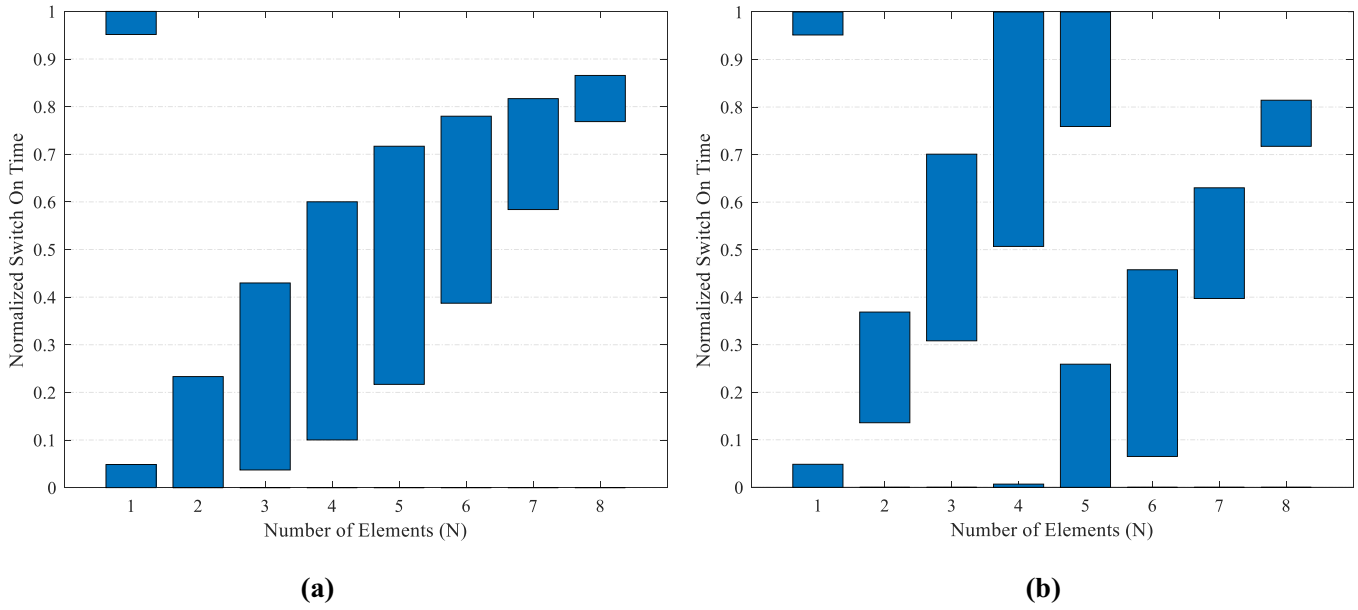


Figure 5. Optimized single-point jammer time schemes for placing deep nulls at (a) 40°, 140°, and (b) 60°, 120°.

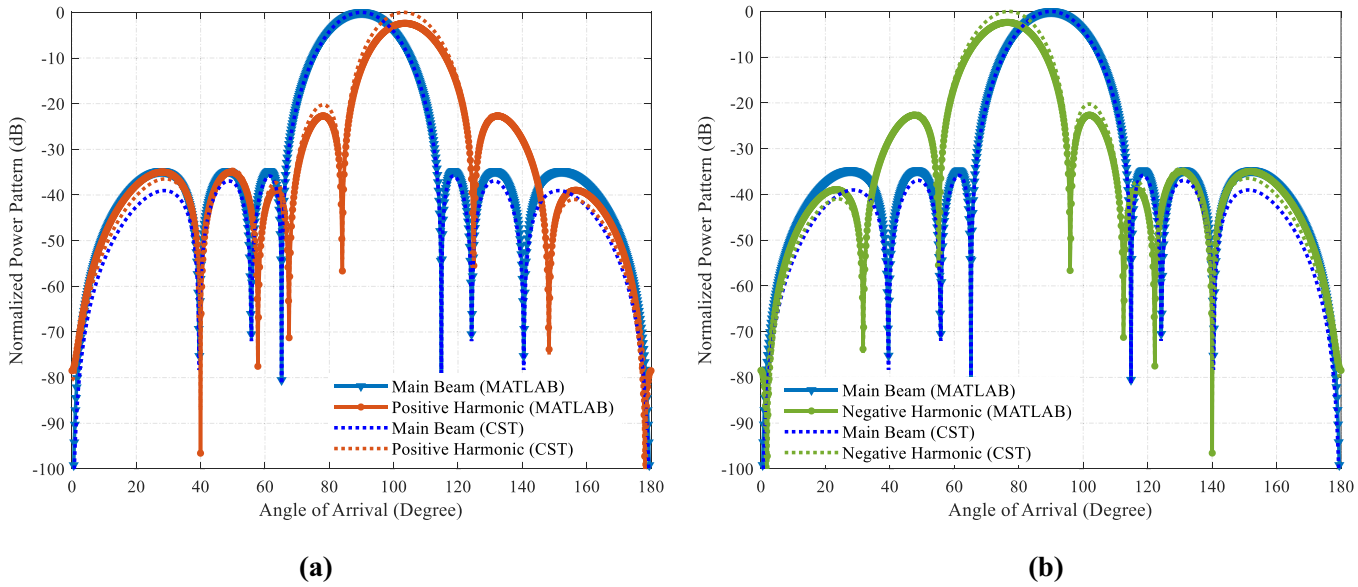


Figure 6. Jamming with deep nulls at (a) 40° using the positive harmonics and (b) 140° using the negative harmonics.

objective function, and the radiated power in higher sidebands up to 10 harmonics is calculated by using the closed-form sideband power equation derived in equation (22). The main beam and the first harmonics consume the largest portions of the total radiated power, i.e., 39.9% and 20.8%, respectively. The radiation power efficiency of the scanned patterns in the time-modulated sidelobe canceller beam scanner is 81.5%, and the total wasted power in higher harmonics is 18.5%. The other radiation properties, such as the half-power beam widths (HPBWs) of the main beams, are reported as 17.4° for all three cases. The HPBWs for the ±15°, ±30°, and ±45° scanned beams of all the three cases are reported as 16.4°, 18.5°, and 23.6°, respectively. The directivities for all the cases are measured as 8.5 dB. The analysis shows that an efficient time-modulated sidelobe-canceller beam scanner is designed in this research to address the much-needed radiation performance requirements for radars. The SPST RF switches used to implement the proposed switching scheme for beam-scanning applications also incur losses in a practical scenario, depending on the ON and OFF timings of the switches. The RF switching efficiency for SPST switches can be calculated as the ratio of the sum of the total ON time to the overall ON and OFF time within the modulation period [27]. The RF switching efficiency for beam scanning is calculated as 61.2%.

Single-point time-modulated jammer

The adaptability of the time-modulated beamformer is further tested to meet the advanced radar requirements, such as steering the strategic nulls toward jammers. The idea is to point a zero-signal space into the angular region so that interfering signals

https://doi.org/10.1017/S1759078726103195 Published online by Cambridge University Press

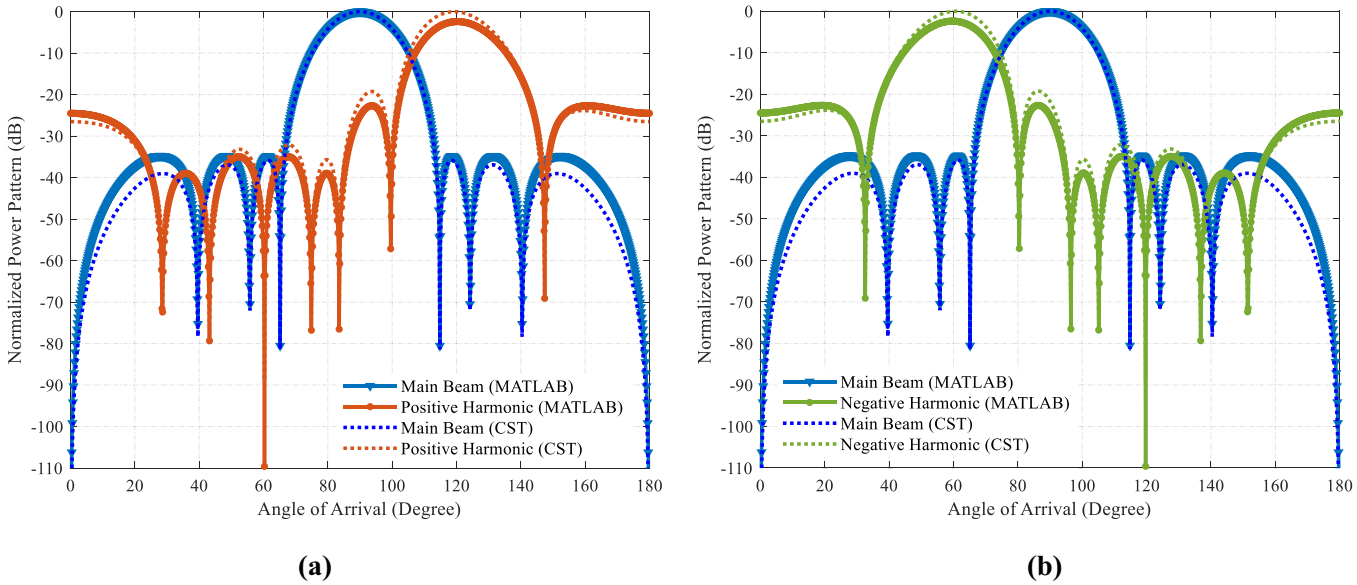


Figure 7. Jamming with deep nulls at (a) 60° using the positive harmonics and (b) 120° using the negative harmonics.

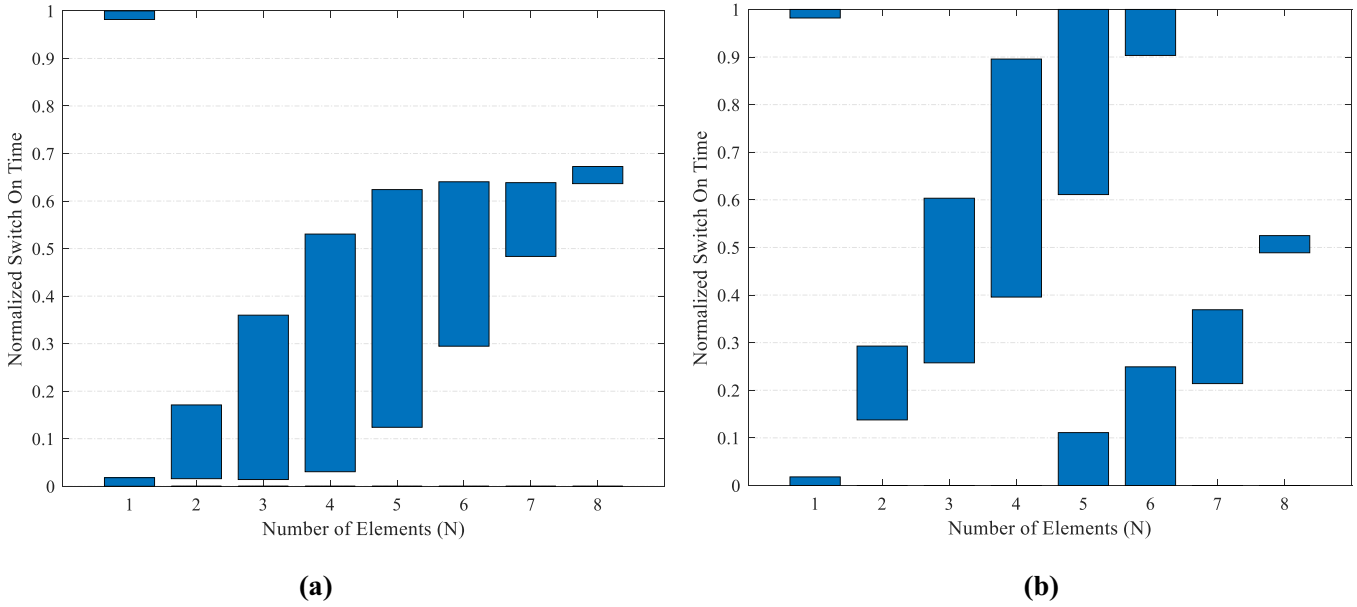


Figure 8. Optimized sectoral jammer timings to suppress (a) 0° to 65° and 115° to 180°, (b) 40° to 80° and 100° to 140°.

in this region can be blocked. The normalized time scheme for the beamformer is designed to place single nulls by scanning the first-harmonic beams of the 8-element array for jamming mitigation. The first case of a single-point jammer with the first harmonics is targeted by producing zero-signal regions at 40° and 140°. Similarly, the second case of a single-point jammer aims to place single nulls at 60° and 120° using the symmetric first-order harmonics on both sides of the main beam pattern. In Case 1, the optimal time scheme for the proposed single-point jamming beamformer is aimed to place null points at 40° and 140°, as shown in Fig. 5(a), and the optimal pulse scheme for the second case for placing nulls toward 60° and 120°, is depicted in Fig. 5(b). The corresponding radiation patterns for a single-point anti-jammer are shown in Figs. 6 and 7. In Fig. 6(a), the first positive harmonic is scanned such that a deep null of −98.5 dB is obtained at 40°. Similarly, the first negative harmonic beam also creates a deep null of the same magnitude at 140°, given in Fig. 6(b). For the second case, the single-point jamming beamformer produces the zero-signal regions by placing deep nulls with −110 dB magnitude at 60° and 120° using the first positive and first negative harmonic beam patterns. The single-point jamming performances of Case 2 with the positive and negative harmonic responses are given in Fig. 7(a) and (b), respectively. The main beams are unaltered in the broadside direction. In addition to that, the same level of SLLs, i.e., −34.8 dB and −22.8 dB, is also maintained for the main beam and harmonic beams, respectively. The radiated power in the main beam pattern is 39.9%, and the first harmonic beams consume 20.8% power. The directivities for all the cases are reported as 8.5 dB. The RF switching efficiency for the SPST configurations proposed for the time-modulated single-point jammer is reported

https://doi.org/10.1017/S1759078726103195 Published online by Cambridge University Press

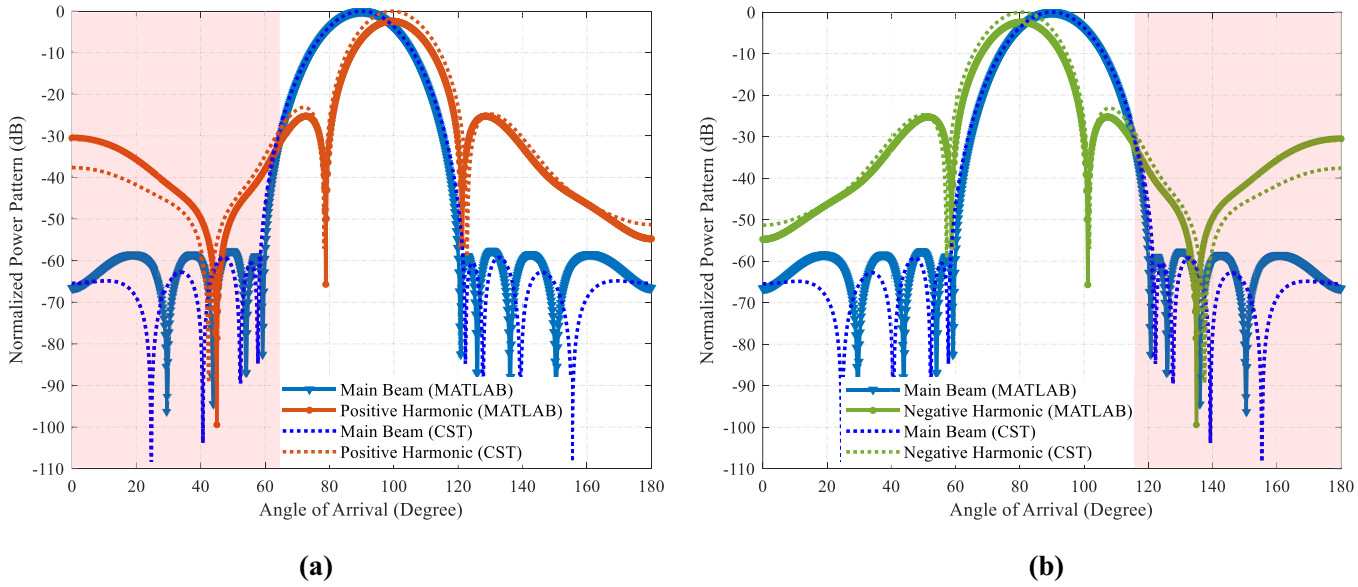


Figure 9. Sectoral jamming patterns to suppress (a) 0° to 65° and (b) 115° to 180° using positive and negative harmonics.

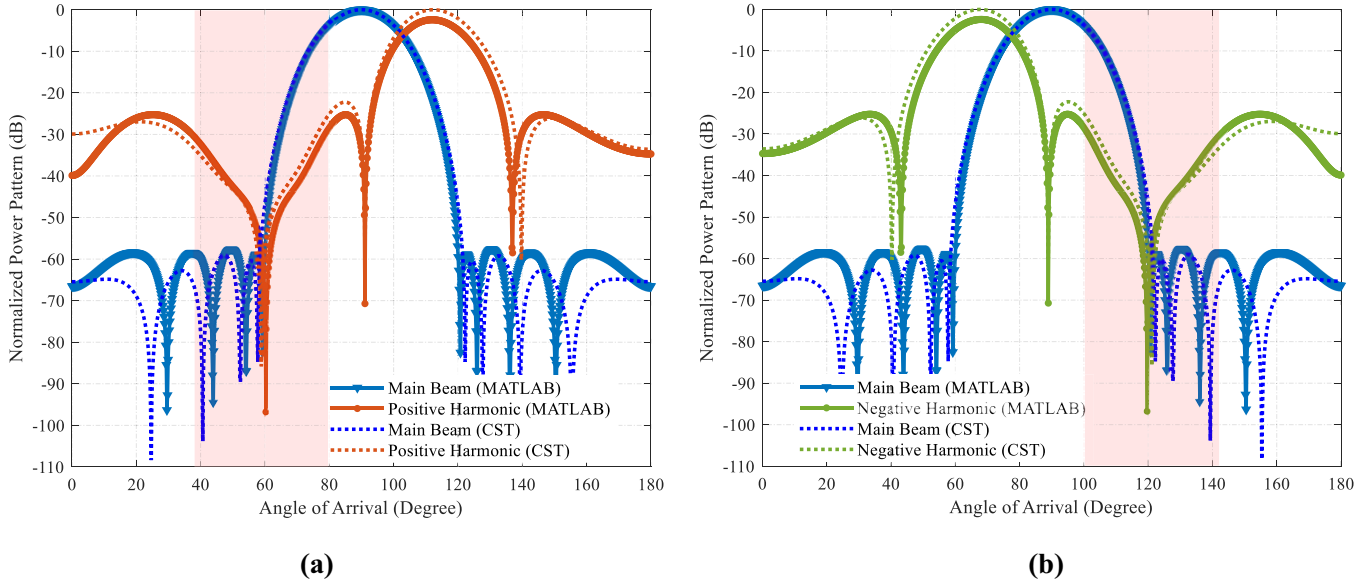


Figure 10. Sectoral jamming patterns to suppress (a) 40° to 80° and (b) 100° to 140° using positive and negative harmonics.

as 61.2%. The radiation patterns simulated using MATLAB software are also cross-validated against the CST Studio-based results for the 8-element dipole antenna arrays. The outcomes have shown close resemblance for the single-point time-modulated anti-jammer application. The proposed sidelobe-canceller beamformer performance for the single-point jammer shows much-needed adaptability and improved reception of the intended signals by blocking the unintended ones.

Sectorized time-modulated jammer

The idea of a time-modulated sidelobe-canceller jammer is further expanded in this section by proposing an adaptable beamformer to suppress interfering signals over a broad region or sector, rather than placing a deep null at a particular point. Two different cases of sectorized jamming are addressed in this research, **where Case 1** deals with sectorized anti-jamming in the regions 0° to 65° and 115° to 180° using the first positive and first negative harmonic beams, respectively. In **Case 2**, the sectorized jamming is aimed to suppress signals in the regions 40° to 80° and 100° to 140° using first-order harmonics. The angular sectors are intended to suppress $\widetilde{SLL}$s below −30 dB for jamming mitigation. The quantum-optimized time schemes for both cases are shown in Fig. 8(a) and (b). The corresponding sectorized jamming patterns for **Case 1** with positive and negative harmonics are presented in Fig. 9(a) and (b). The first positive harmonics shown in Fig. 9(a) indicates that a broad sector from 0° to 68° is suppressed below −30 dB with a deep null of −99.6 dB at 45°. Similarly, the first negative harmonics in Fig. 9(b) provides sectorized jamming in the region of 112° to 180°, where the entire sector is suppressed below −30 dB,

https://doi.org/10.1017/S1759078726103195 Published online by Cambridge University Press

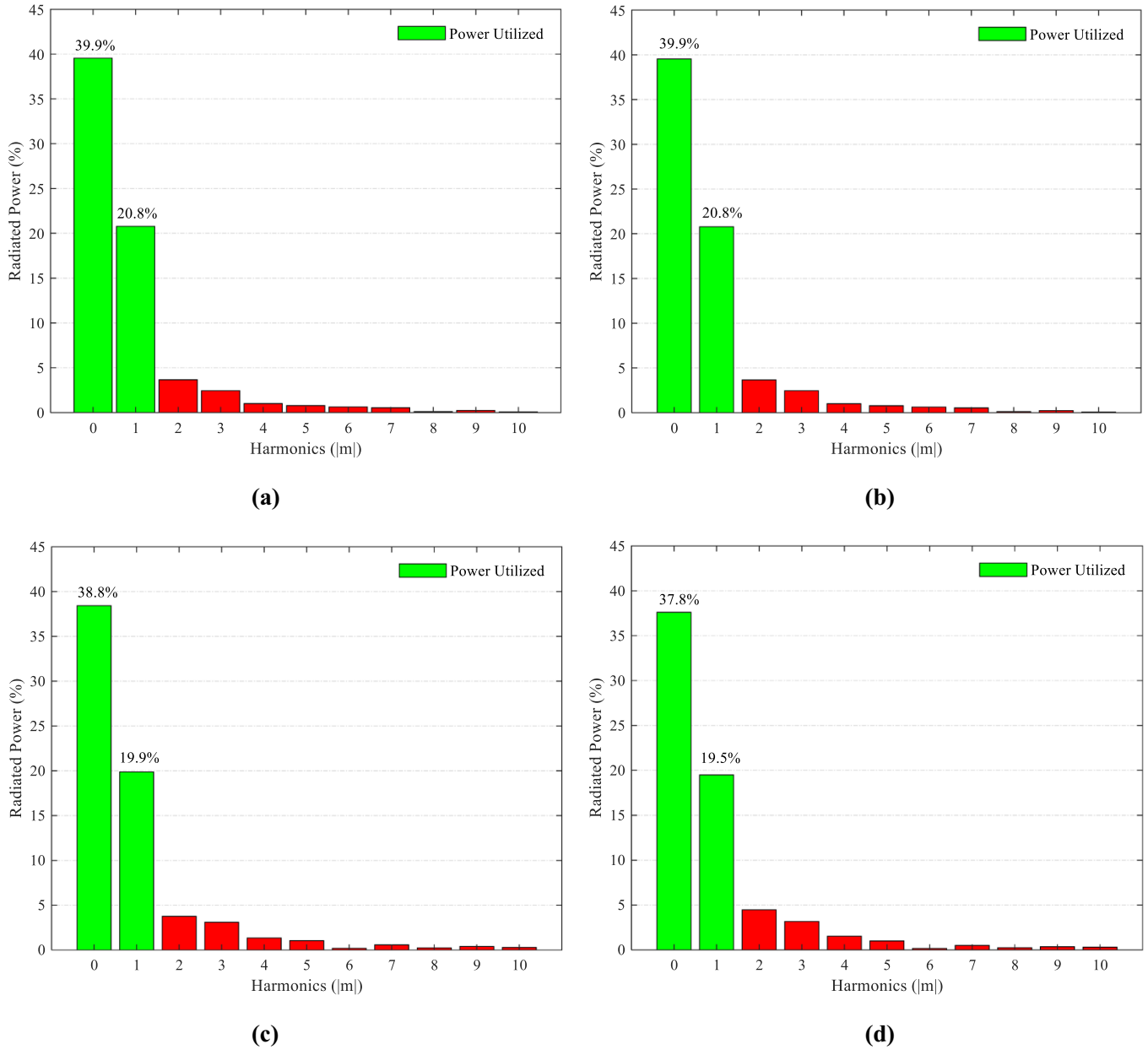


Figure 11. Power consumed by the main beam, first harmonics, and higher harmonics patterns for (a) Sidelobe-canceller beamformer, (b) Beam scanner, (c) Sectoral anti-jammer Case 1, and (d) Sectoral anti-jammer Case 2.

with a symmetric deep null at 135°. For **Case 2**, the first positive harmonics shown in Fig. 10(a) produce a sectorized jamming in the region from 35° to 80°, lowering all the responses in this region below −30 dB with a deep null of −96.9 dB pointed at 60°. The symmetric harmonic patterns given in Fig. 10(b) also show similar sectorized jamming performance in the region of 100° to 145° by pointing a deep null of the same magnitude at 120°. The SLLs of the main beam and first harmonic beams are suppressed as −59.8 and −26.5 dB, which shows a convincing performance over the targeted objective of −20 dB $\widetilde{SLL}$ for interference rejection. The directivities of the array in both cases are reported as 8.2 dB. The sectoral jammer also shows efficient power utilization, with 38.8% and 19.9% of the power consumed by the main beam and each of the first-harmonic patterns, respectively, in **Case 1**. The total power efficiency for the sectorized jamming application in **Case 1** is 78.6%, and the power wasted in higher harmonics is 21.4%. In **Case 2**, the main beam and the first side beams accounts for 37.8% and 19.5% of the total radiated power, respectively. The total power efficiency is measured as 76.8%, and the power wasted in higher harmonics is 23.2%. The power utilized in desired patterns and wasted in higher-order harmonics for all the objectives is shown in Fig. 11. The RF switching efficiency for the SPST configurations proposed in time-modulated sectorized jammer is reported as 51.8%. The radiation patterns simulated in MATLAB are also cross-validated against CST Studio-based results for the 8-element dipole antenna arrays. The outcomes have shown close resemblance for the sectorized time-modulated anti-jammer application.

The comparison of the proposed beamformer outcomes with other state-of-the-art works is also presented in Table 1. The SLL of

https://doi.org/10.1017/S1759078726103195 Published online by Cambridge University Press

Table 1. Comparison of the proposed sidelobe cancelling time-modulated beamformer with other contemporary works

Reference Works	$SLL_{(m=0)}$	$SLL_{(m=\pm1)}$	$P_{(m=0)}$	$P_{(m=\pm1)}$	$P_{(Efficiency)}$	$P_{(Wasted)}$
Poli *et al.* 2011 [6]	−21.6 dB	−20 dB	30.5%	20.7%	71.9%	28.1%
Poli *et al.* 2014 (C1) [22]	−21.7 dB	−20 dB	30.4%	19.3%	69.7%	30.9%
Poli *et al.* 2011 (C2) [22]	−21.2 dB	−20 dB	31.5%	19.9%	71.2%	28.7%
Tan *et al.* 2021 [24]	−20 dB	−23.6 dB	*Na	*Na	*Na	*Na
Gassab *et al.* 2019 (C1) [34]	−30 dB	−12 dB	*Na	*Na	*Na	*Na
Gassab *et al.* 2019 (C2) [34]	−18.9 dB	−23.8 dB	*Na	*Na	*Na	*Na
Ram *et al.* 2021 (C1) [35]	−15.9 dB	−15.9 dB	*Na	*Na	*Na	*Na
Ram *et al.* 2021 (C2) [35]	−17.7 dB	−17.7 dB	*Na	*Na	*Na	*Na
Ram *et al.* 2021 (C3) [35]	−14.9 dB	−14.9 dB	*Na	*Na	*Na	*Na
Ram *et al.* 2021 (C4) [35]	−18.2 dB	−18.2 dB	*Na	*Na	*Na	*Na
Bhattacharya *et al.* 2017 (C1) [50]	−18.3 dB	−18.4 dB	*Na	*Na	*Na	*Na
Bhattacharya *et al.* 2017 (C2) [50]	−22.4 dB	−22.2 dB	*Na	*Na	*Na	*Na
Proposed Beamformer (This work)	−59.8 dB	−26.5 dB	38.8%	19.9%	78.6%	21.4%

*C1, C2, C3, C4 – Different Cases; *Na – Not available

the main beam pattern has improved to −59.8 dB. The SLL for the anti-jamming first-harmonic beams is −26.5 dB, compared to the best-reported result of −23.8 dB. The overall power efficiency has also shown superior performance with 78.6% compared to 71.28% reported in Table 1. From detailed analysis, it is proven that an efficient and adaptive sidelobe-canceller beamformer is designed in this research which is capable of electronic beam scanning, sidelobe cancellation, placing single nulls for single-point jamming, and suppression of signals for sectoral jamming mitigation useful for radars.

Conclusion

The research proposes the design of an efficient time-modulated sidelobe-canceller beamformer array for advanced radar applications by emphasizing and exploring the electronic beam scanning, null placing, and jamming mitigation capabilities. Scanning patterns toward prespecified directions is a crucial requirement for modern radars, enabling the accurate tracking of an object or intended signals. The associated challenges, such as sidelobe suppression while maintaining the radiation efficiencies of the beam patterns, are also addressed in this research. Furthermore, optimal time-scheme frameworks have been developed to provide jamming mitigation characteristics in the desired directions. A complete mathematical model of the switching schemes required to achieve the objectives in an 8-element time-modulated array is proposed. In addition to that, the mathematical modeling of the shifted switching scheme, responsible for a cumulative phase divergence performance, is also presented in this research. The proposed sidelobe-canceller beamformer achieves decent scanning coverage of around 90° in the broadside direction. The simultaneous harmonic beams of the time-modulated beamformer also ensure good sidelobe suppression properties by maintaining below −30 dB sidelobe levels (SLLs) for all the proposed applications. The SLLs of the harmonic patterns are also suppressed along with the main beam, suggesting a simple beamforming network that can affect all harmonics and the desired beams simultaneously. The electronic beam-scanning performance shows that the first negative and positive harmonics are utilized to scan at multiple prespecified directions, including 45°, 60°, 75°, 105°, 120°, and 135°. The broad scan coverage from 45° to 135°, with sidelobes below −34.8 dB and −22.8 dB for interference rejection, is useful for scanning radars. Further, single-point jammers are targeted by placing null points in the angle of arrival, and the results show the jamming performance of the proposed single-point jammers at 40°, 60°, 120°, and 140° with desired sidelobe suppression. The idea is further expanded to sectorized jamming, where specific regions such as 0° to 65°, 40° to 80°, 100° to 140°, and 115° to 180° are targeted to suppress signals below the desired level blocking transmission or reception in those sectors. The overall sidelobes of the main beam and the harmonic beams are also lowered to −59.8 dB and −26.5 dB. The radiation power efficiencies of all the proposed applications also show that around 80% of the power is utilized for scanning and jamming applications. The proposed results are also compared with the state-of-the-art research to show their superior performance. This research proposes and explores time-modulated beamforming antenna arrays capable of simultaneous electronic beam scanning and jamming mitigation, with sidelobe reduction characteristics.

Data availability statement. No new data are created or analyzed during the work. The sharing of data is not applicable for this article.

Competing interests. The authors hereby declare that they do not have any competing financial or personal interests.

References

1. **Maneiro-Catoira R, Brégains J, García-Naya J and Castedo L** (2017) Time modulated arrays: From their origin to their utilization in wireless communication systems. *Sensors* **17**, 590. https://doi.org/10.3390/s17030590
2. **Rocca P, Yang F, Poli L and Yang S** (2019) Time-modulated array antennas – Theory, techniques, and applications. *Journal of Electromagnetic Waves and Applications* **33**, 1503–1531. https://doi.org/10.1080/09205071.2019.1627251

3. **Tong Y and Tennant A** (2012) A two-channel time modulated linear array with adaptive beamforming. *IEEE Transactions on Antennas and Propagation* **60**, 141–147. https://doi.org/10.1109/TAP.2011.2167936
4. **Li H, Chen Y and Yang S** (2021) Design and analysis of an amplitude-phase weighting module for harmonic beamforming in time-modulated antenna arrays. *AEU - International Journal of Electronics and Communications* **138**, 153835. https://doi.org/10.1016/j.aeue.2021.153835
5. **Yang S, Gan YB, Qing A and Tan PK** (2005) Design of a uniform amplitude time modulated linear array with optimized time sequences. *IEEE Transactions on Antennas and Propagation* **53**, 2337–2339. https://doi.org/10.1109/TAP.2005.850765
6. **Poli L, Rocca P, Oliveri G and Massa A** (2011) Harmonic beamforming in time-modulated linear arrays. *IEEE Transactions on Antennas and Propagation* **59**, 2538–2545. https://doi.org/10.1109/TAP.2011.2152323
7. **Bregains JC, Fondevila-Gomez J, Franceschetti G and Ares F** (2008) Signal radiation and power losses of time-modulated arrays. *IEEE Transactions on Antennas and Propagation* **56**, 1799–1804. https://doi.org/10.1109/TAP.2008.923345
8. **Shanks H** (1961) A new technique for electronic scanning. *IRE Transactions on Antennas and Propagation* **9**, 162–166. https://doi.org/10.1109/TAP.1961.1144965
9. **Li G, Yang S, Chen Y and Nie Z-P** (2009) A novel electronic beam steering technique in time modulated antenna array. *PIER* **97**, 391–405. https://doi.org/10.2528/PIER09072602
10. **Yang S, Gan YB and Tan PK** (2004) Comparative study of low sidelobe time modulated linear arrays with different time schemes. *Journal of Electromagnetic Waves and Applications* **18**, 1443–1458. https://doi.org/10.1163/1569393042954910
11. **Ma Y, Miao C, Li Y and Wu W** (2020) Time-modulated sparse linear array synthesis with minimum elements and a specific sidelobe. *The Institution of Engineering and Technology Microwaves, Antennas & Propagation* **14**, 1595–1598. https://doi.org/10.1049/iet-map.2020.0459
12. **Poddar S, Paul P, Chakraborty A, Ram G and Mandal D** (2022) Design optimization of linear arrays and time-modulated antenna arrays using meta-heuristics approach. *International Journal of Numerical Modelling* **35**, e3010. https://doi.org/10.1002/jnm.3010
13. **Maneiro-Catoira R, Bregains JC, Garcia-Naya JA and Castedo L** (2017) Enhanced time-modulated arrays for harmonic beamforming. *IEEE Journal of Selected Topics in Signal Processing* **11**, 259–270. https://doi.org/10.1109/JSTSP.2016.2627178
14. **Zhu Q, Yang S, Yao R and Nie Z** (2012) Gain improvement in time-modulated linear arrays using SPDT switches. *IEEE Antennas and Wireless Propagation Letters* **11**, 994–997. https://doi.org/10.1109/LAWP.2012.2213292
15. **Chen J, Liang X, He C, Fan H, Zhu W, Jin R and Geng J** (2017) Efficiency improvement of time modulated array with reconfigurable power divider/combiner. *IEEE Trans Antennas Propagat* **65**, 4027–4037. https://doi.org/10.1109/TAP.2017.2712811.
16. **Yang S, Gan YB and Qing A** (2002) Sideband suppression in time-modulated linear arrays by the differential evolution algorithm. *IEEE Antennas and Wireless Propagation Letters* **1**, 173–175. https://doi.org/10.1109/LAWP.2002.807789
17. **Aksoy E and Afacan E** (2014) A comparative study on sideband optimization in time-modulated arrays. *International Journal of Antennas and Propagation* **2014**, 1–14. https://doi.org/10.1155/2014/290737
18. **Poli L, Rocca P, Manica L and Massa A** (2010) Handling sideband radiations in time-modulated arrays through particle swarm optimization. *IEEE Transactions on Antennas and Propagation* **58**, 1408–1411. https://doi.org/10.1109/TAP.2010.2041165
19. **Poli L, Rocca P, Manica L and Massa A** (2010) Time modulated planar arrays – Analysis and optimisation of the sideband radiations. *IET Microwaves, Antennas & Propagation* **4**, 1165–1171. https://doi.org/10.1049/iet-map.2009.0379
20. **Poli L, Rocca P and Massa A** (2012) Sideband radiation reduction exploiting pattern multiplication in directive time-modulated linear arrays. *IET Microwaves, Antennas & Propagation* **6**, 214–222. https://doi.org/10.1049/iet-map.2011.0159
21. **Poli L, Rocca P, Manica L and Massa A** (2010) Pattern synthesis in time-modulated linear arrays through pulse shifting. *IET Microwaves, Antennas & Propagation* **4**, 1157–1164. https://doi.org/10.1049/iet-map.2009.0042
22. **Poli L, Moriyama T and Rocca P** (2014) Pulse splitting for harmonic beamforming in time-modulated linear arrays. *International Journal of Antennas and Propagation* **2014**, 1–9. https://doi.org/10.1155/2014/797590
23. **Zhu Q, Yang S, Yao R, Huang M and Nie Z** (2013) Unified time- and frequency-domain study on time-modulated arrays. *IEEE Transactions on Antennas and Propagation* **61**, 3069–3076. https://doi.org/10.1109/TAP.2013.2253538
24. **Tan J, Hu J, Dong X, Li H and Zhou J** (2021) Research on pattern synthesis of time modulated sparse array based on discrete variable convex optimization. *Wireless Communications and Mobile Computing* **2021**, 6622168. https://doi.org/10.1155/2021/6622168
25. **Chakraborty A, Ram G and Mandal D** (2020) Optimal pulse shifting in timed antenna array for simultaneous reduction of sidelobe and sideband level. *IEEE Access* **8**, 131063–131075. https://doi.org/10.1109/ACCESS.2020.3010047
26. **Chakraborty A, Ram G and Mandal D** (2022) Time-modulated linear array synthesis with optimal time schemes for the simultaneous suppression of sidelobe and sidebands. *International Journal of Microwave and Wireless Technologies* **14**, 768–780. https://doi.org/10.1017/S175907872100088X
27. **Chakraborty A, Ram G and Mandal D** (2021) Pattern synthesis of timed antenna array with the exploitation and suppression of harmonic radiation. *International Journal of Communication* **34**, e4727. https://doi.org/10.1002/dac.4727
28. **Yang S, Gan YB and Peng Khiang T** (2003) A new technique for power-pattern synthesis in time-modulated linear arrays. *IEEE Antennas and Wireless Propagation Letters* **2**, 285–287. https://doi.org/10.1109/LAWP.2003.821556
29. **Aksoy E and Afacan E** (2010) Thinned nonuniform amplitude time-modulated linear arrays. *IEEE Antennas and Wireless Propagation Letters* **9**, 514–517. https://doi.org/10.1109/LAWP.2010.2051312
30. **Zhu Q, Yang S, Zheng L and Nie Z** (2012) Design of a low sidelobe time modulated linear array with uniform amplitude and sub-sectional optimized time steps. *IEEE Transactions on Antennas and Propagation* **60**, 4436–4439. https://doi.org/10.1109/TAP.2012.2207082
31. **Chakraborty A, Singh I, Gupta S, Ram G and Mandal D** (2023) Sideband power control in Time-Modulated antenna arrays for bidirectional harmonic beamforming and beam scanning. *AEU - International Journal of Electronics and Communications* **170**, 154788. https://doi.org/10.1016/j.aeue.2023.154788
32. **Chakraborty A, Ram G and Mandal D** (2021) Multibeam steered pattern synthesis in time-modulated antenna array with controlled harmonic radiation. *International Journal of RF and Microwave Computer-Aided Engineering* 31. https://doi.org/10.1002/mmce.22597
33. **Chakraborty A, Ram G and Mandal D** (2021) Time-modulated multi-beam steered antenna array synthesis with optimally designed switching sequence. *International Journal of Communication* **34**, e4828. https://doi.org/10.1002/dac.4828
34. **Gassab O, Azrar A, Dahimene A, Bouguerra S and He C** (2020) Efficient electronic beam steering method in time modulated linear arrays. *The Institution of Engineering and Technology Microwaves, Antennas & Propagation* **14**, 402–408. https://doi.org/10.1049/iet-map.2019.0673
35. **Ram G** (2021) Multi-beam steered harmonic pattern synthesis in timed antenna array with optimized and pre-defined RF switching. *International Journal of Numerical Modelling* **34**, e2912. https://doi.org/10.1002/jnm.2912
36. **Chakraborty A, Ram G and Mandal D** (2022) Power pattern synthesis of a moving phase center time modulated antenna array using symmetrically and asymmetrically positioned time schemes. *International Journal of RF and Microwave Computer-Aided Engineering* 32. https://doi.org/10.1002/mmce.23442
37. **Chakraborty A, Ram G and Mandal D** (2023) Phase center motion-based time modulated arrays with preprocessed time schemes for selective harmonic beamforming in B5G communication systems. *Transactions on*

https://doi.org/10.1017/S1759078726103195 Published online by Cambridge University Press

Emerging Telecommunications Technologies **34**, e4754. https://doi.org/10.1002/ett.4754

38. **Yang S, Gan YB and Tan PK** (2005) Linear antenna arrays with bidirectional phase center motion. *IEEE Transactions on Antennas and Propagation* **53**, 1829–1835. https://doi.org/10.1109/TAP.2005.846754
39. **He C, Yi G, Chen J, Zhu W, Liang X, Geng J and Jin R** (2019) A novel radar based on two-element time-modulated array. *IEEE Geoscience and Remote Sensing Letters* **16**, 524–528. https://doi.org/10.1109/LGRS.2018.2877973
40. **Gang L, Yang S and Nie Z** (2010) Direction of arrival estimation in time modulated linear arrays with unidirectional phase center motion. *IEEE Transactions on Antennas and Propagation* **58**, 1105–1111. https://doi.org/10.1109/TAP.2010.2041313
41. **Rocca P, Manica L, Poli L and Massa A** (2009) Synthesis of compromise sum-difference arrays through time-modulation. *Institution of Engineering and Technology Radar, Sonar & Navigation* **3**, 630–637. https://doi.org/10.1049/iet-rsn.2009.0058
42. **Rocca P, Poli L, Oliveri G and Massa A** (2011) Synthesis of sub-arrayed time modulated linear arrays through a multi-stage approach. *IEEE Transactions on Antennas and Propagation* **59**, 3246–3254. https://doi.org/10.1109/TAP.2011.2161535
43. **Chakraborty A, Ram G and Mandal D** (2023) Time modulation based unconventional phased antenna arrays for monopulse and multifunction radar systems. *International Journal of Numerical Modelling* **36**, e3074. https://doi.org/10.1002/jnm.3074
44. **Poli L, Rocca P, Oliveri G and Massa A** (2011) Adaptive nulling in time-modulated linear arrays with minimum power losses. *IET Microwaves, Antennas & Propagation* **5**, 157–166. https://doi.org/10.1049/iet-map.2010.0015
45. **Chakraborty A, Mishra A, Singh I, Ahmad S, Khan MJ, Sharma D, Alkhayyat A and Gupta S** (2024) Optimal design of smart antenna arrays for beamforming, direction finding, and null placement using the soft computing method. *International Journal of Numerical Modelling* **37**, e3302. https://doi.org/10.1002/jnm.3302
46. **Chakraborty A, Saxena RS, Verma A, Juyal A, Gupta S, Singh I, Ram G and Mandal D** (2024) Multi-pattern synthesis in fourth-dimensional antenna arrays using BGM-based quasi-Newton memetic optimization method. *International Journal of Microwave and Wireless Technologies* **16**, 284–294. https://doi.org/10.1017/S1759078723000910
47. **Chakraborty A, Singh I, Bhattacharya S, Sharma KP, Namdev V, Shukla AK, Alkhayyat A and Shah SK** (2024) Multiple pattern synthesis in four-dimensional antenna arrays using the Quasi-Newton Memetic optimization method. *IETE Journal of Research* **70**, 6055–6068. https://doi.org/10.1080/03772063.2023.2294867
48. **Li G, Yang S, Huang M and Nie Z** (2010) Shaped patterns synthesis in time-modulated antenna arrays with static uniform amplitude and phase excitations. *Frontiers of Electrical and Electronic Engineering in China* **5**, 179–184. https://doi.org/10.1007/s11460-010-0005-2
49. **Rocca P, Zhu Q, Bekele ET, Yang S and Massa A** (2014) 4-D arrays as enabling technology for cognitive radio systems. *IEEE Transactions on Antennas and Propagation* **62**, 1102–1116. https://doi.org/10.1109/TAP.2013.2288109
50. **Bhattacharya R, Saha S and Bhattacharyya TK** (2017) Mutated IWO optimized 4-D array for femtocell cognitive radio. *IEEE Antennas and Wireless Propagation Letters* **16**, 2614–2617. https://doi.org/10.1109/LAWP.2017.2735999
51. **Alorf A** (2023) A survey of recently developed metaheuristics and their comparative analysis. *Engineering Applications of Artificial Intelligence* **117**, 105622. https://doi.org/10.1016/j.engappai.2022.105622
52. **Robinson J and Rahmat-Samii Y** (2004) Particle swarm optimization in electromagnetics. *IEEE Transactions on Antennas and Propagation* **52**, 397–407. https://doi.org/10.1109/TAP.2004.823969
53. **Eberhart YS** (2001) Particle swarm optimization: Developments, applications and resources. In *Proceedings of the 2001 Congress on Evolutionary Computation (IEEE Cat. No.01TH8546)*, vol. 1, Seoul, South Korea: IEEE, pp. 81–86. https://doi.org/10.1109/CEC.2001.934374.
54. **Sun J, Feng B and Wenbo X** (2004) Particle swarm optimization with particles having quantum behavior. In *Proceedings of the 2004 Congress on Evolutionary Computation (IEEE Cat. No.04TH8753)*, Portland, OR, USA: IEEE, pp. 325–331. https://doi.org/10.1109/CEC.2004.1330875.
55. **Agrawal RK, Kaur B and Agarwal P** (2021) Quantum inspired Particle Swarm Optimization with guided exploration for function optimization. *Applied Soft Computing* **102**, 107122. https://doi.org/10.1016/j.asoc.2021.107122

https://doi.org/10.1017/S1759078726103195 Published online by Cambridge University Press